NUMERICAL STUDIES OF BOTTOM SHEAR STRESS AND SEDIMENT DISTRIBUTION ON THE AMAZON CONTINENTAL SHELF

PAUL W. JEWELL[1], ROBERT F. STALLARD[2], AND GEORGE L. MELLOR[3]

[1] Dept. of Geology and Geophysics, University of Utah, Salt Lake City, UT 84112 USA

[2] United States Geological Survey, Denver, CO 80225 USA

[3] Program in Atmospheric and Oceanic Sciences, Princeton University, Princeton, NJ 08544 USA

ABSTRACT: The relation between bottom shear stress and the distribution of bottom sediments on the Amazon continental shelf has been studied using a three-dimensional, primitive-equation computer model that incorporates the turbulence-closure scheme of Mellor and Yamada (1982) for calculating eddy diffusivity and a simple algorithm for computing nonlinear wave-current influences on bottom shear stress. Model results compare reasonably well with salinity data sets for the Amazon plume. Model results on distribution of bottom currents and bottom shear stresses help explain some of the observed sedimentological features of the Amazon continental shelf. High concentrations of suspended sediment in the Amazon River are transported outward over the continental shelf and northward by the North Brazil Coastal Current. As this sediment settles out of the water column, it forms the prograding, subaqueous delta described by Nittrouer et al. (1986). Accumulation rates are greatest shoreward of the 40-m isobath due to a zone of convergent, cross-shelf residual tidal velocities. Little sediment is deposited in the shallow parts of the shelf, where bottom shear stress exceeds 10 dynes/cm² over a diurnal tidal cycle. Zones of laminated sand and mud on the Amazon continental shelf coincide with areas of high interseasonal differences in bottom shear stress. Our results suggest that our model may be useful in interpreting sedimentation in ancient sedimentary basins as well.

INTRODUCTION

Estuaries represent a transition from terrestrial to marine settings and as such, typically act as repositories for continentally derived sediment. Estuarine environments are commonly less energetic than fluvial environments, and therefore the river sediment load tends to be deposited when it enters the more saline parts of the estuary. Moreover, flocculation of suspended river sediment is often favored by the high ionic strength of seawater.

The sequestering of sediment in estuaries is significant on geological time scales. During high stands of sea level, seawater covers continental shelves and occupies former river valleys along coastal plains. These drowned river valleys often act as depocenters for large volumes of sediment. Large, sediment-laden rivers like the Amazon and Yangtze tend to deposit sediment over vast areas of the continental shelf. During low stands of sea level, much of the sediment in drowned river valleys and on the continental shelves is exported to the deep ocean.

Knowledge of the exact nature of sediment movement and accumulation in estuaries and on continental shelves is hindered by the lack of detailed observations. Tidally dominated estuaries, like those on the eastern seaboard of the United States, occupy relatively small areas and have been studied in considerable detail (e.g., Nelson 1972). Large rivers like the Amazon, Yangtze, and Ganges–Brahmaputra deposit sediment over hundreds of square kilometers. Outflow from these large rivers often extends over the continental shelf and for this reason are typically referred to as plumes rather than estuaries (e.g., Edmond et al. 1981). These large river systems contribute much of the global sediment yield (Milliman and Meade 1983) and are therefore critical to understanding the global sediment cycle. Unfortunately, these major dispersal systems are often poorly understood because the time scale required to cross and sample a major river plume greatly exceeds the time scale of important sedimentological and geological processes. Moreover, formidable logistical problems must be surmounted to study these systems, many of which are located away from the major research centers.

An important adjunct to direct, detailed observations of large sediment-dispersal systems is a physically based computer model with well constrained boundary conditions. Such models offer advantages of complete coverage of an entire system and the possibility of examining the effects of specific parameters (e.g., tides and winds) on sediment dispersal. A realistic, physically based computer model can pinpoint specific areas or processes that should be emphasized by field programs. Such models can also be used to establish the spatial and temporal context of specific samples taken within a large, rapidly changing system.

Considerable effort has been directed toward prognostic equations and models capable of predicting bottom shear stress and sediment transport. Summaries of some of these equations are given by Yalin (1977), Middleton and Southard (1984), and Dyer (1986). The advent of large, array-processing computers has allowed fluid-circulation models to be coupled with some of these sediment-transport equations. Studies of this kind include those by Sheng and Lick (1979) and Graber et al. (1989). In recent years, sedimentologists and fluid dynamicists alike have come to recognize that the combination of waves and currents has a great effect on the dynamics of bottom shear stress (Smith 1977; Grant and Madsen 1979). Studies that have integrated wave-current theories with field data include those of Wiberg and Smith (1983), Grant et al. (1984), Drake and Cacchione (1986), and Davies et al. (1988).

This study represents an initial attempt to couple simplified equations describing dynamics of bottom shear stress under combined wave-current flow to a sophisticated, three-dimensional fluid-dynamic computer model of estuarine and coastal circulation. The Amazon continental shelf was chosen for this study for several reasons. (1) The Amazon plume exerts considerable influence on sedimentation over much of the continental shelf of northeastern South America (Nittrouer et al. 1986). (2) The vast size of the Amazon dispersal system makes synoptic observations of flow and sedimentation difficult. (3) The Amazon continental shelf is an excellent example of interglacial sediment storage along a continental margin. Sediment derived from continental weathering (mainly in the Andes Mountains) is being deposited rapidly (up to 10 cm/yr) in a subaqueous delta (Kuehl et al. 1986). (4) Sediment transport and deposition in this large dispersal system are probably similar to other dispersal systems in the modern ocean as well as the geologic past.

AMAZON CONTINENTAL SHELF SEDIMENTATION

Sediment delivered by the Amazon River to the continental shelf is dispersed by the strong, northwestward-flowing North Brazil Coastal Current. The mixing zone has the form of a plume of fresher water that is entrained by the North Brazil Coastal Current. Amazon River sediments are being deposited as far north as the Orinoco River delta (Van Andel 1967) and possibly even the Caribbean Sea (Bowles and Fleischer 1985). Active sedimentation extends as far as 200 km seaward of the river mouth and for several hundred kilometers along the shelf. Accretion of fine-

grained siliciclastic sediment to the Guiana coast began in Miocene time when the Andes Mountains began to rise (Krook 1979). During stands of low sea level, the sediment load of the Amazon is diverted onto the continental slope, where it adds to the Amazon Cone, a major sedimentary feature of the abyssal plain of the Atlantic Ocean (Damuth 1977; Damuth and Kumar 1975).

The modeling domain of this study (Fig. 1) was selected to encompass major sedimentary features of the depositional system. Two general regions of the seabed can be distinguished. The outer-shelf sediments are mostly relict sands from the last low stand of sea level. Shoreward of the 60-m isobath the sediments are mostly fine muds and silts. They were once considered to be relicts from the last marine transgression (12–18 ka) (e.g., Milliman et al. 1975b), but it is now generally accepted that they represent a prograding subaqueous delta that began forming after the end of the last ice age (Nittrouer et al. 1986). Sediment accumulation rates are moderate (on the order of 1 cm/yr) on the inner part of the delta and greatest (> 10 cm/yr) around the 60-m isobath (Kuehl et al. 1986). Much of the delta is characterized by a layer of sediment (up to 2 m thick) that has been intensely reworked by tides and surface-wave shoaling (Kuehl et al. 1986). Large, intense storms do not influence sedimentation beneath the Amazon plume, because river discharge is at the Equator (Fig. 1). The intense physical reworking of sediments prevents establishment of a macrobenthic community (Aller and Aller 1986).

Transport and deposition of suspended sediments in the Amazon dispersal system are strongly influenced by circulation, seabed shear stresses, and salinity. The concentration of suspended sediment in the river mouth is 50–200 mg/kg (Gibbs 1967; Milliman et al. 1975a; Sholkovitz and Price 1980). Concentrations are higher just outside the river mouth due to turbidity associated with the shallow, transverse bar in this area (Fig. 1; Gibbs 1976). Suspended-sediment concentration diminishes to around 1 mg/kg at seawater salinities. Biological activity (mainly diatom production) commences where surface concentrations of suspended sediment decrease to about 10 mg/kg (DeMaster et al. 1986). Approximately 50% of the sediment delivered by the river is being sequestered in the subaqueous delta (Kuehl et al. 1986).

MODEL DESCRIPTION

The three-dimensional fluid-flow model in this study uses conservation equations for momentum, heat, and salt in conjunction with the level 2-1/2 turbulence-closure scheme of Mellor and Yamada (1982). The model belongs to a class of models that address mesoscale phenomena, i.e., those on spatial scales of 1–100 km and time scales of days to months. The turbulence-closure scheme is necessary to accurately compute eddy viscosity and diffusivity terms, which are critical components of the conservation equations. The Mellor-Yamada turbulence-closure scheme computes all components of the Reynolds-stress tensor and contains no adjustable parameters. The exact forms of the governing equations, the turbulence-closure procedure, and numerical implementation are lengthy and not given here; see Blumberg and Mellor (1987) for details.

The three-dimensional version of the Mellor-Yamada model has been used effectively to study a variety of coastal, estuarine, and open-marine settings (Oey et al. 1985b; Mellor and Kantha 1989; Galperin and Mellor 1990). In all of these studies, model output compares favorably with field data. In this paper we concentrate on two specific aspects of Amazon shelf sedimentation: calculations of bottom shear stress and the nature of bottom sediments. In this initial study we do not attempt to model the erosion and deposition of seabed sediments *per se*.

Model Domain

The model domain for the Amazon simulations consists of a 35 × 85 horizontal grid oriented so that the long direction parallels the South American coast (Fig. 1). Cross-shore and along-shore grid spacing is 7.8 km. The model domain therefore covers approximately 270 km in the cross-shore direction and 660 km along shore. Maximum water depth (100 m) is in the extreme northern corner of the domain.

River water enters the model domain at three points along the western boundary (Fig. 1). From north to south these rivers are the North Channel of the Amazon, the South Channel of the Amazon, and Pará River. Although the discharge of the Pará is at least an order of magnitude smaller than that of the Amazon, it may have some impact on the budget of sediments and dissolved chemical species in the plume (Key et al. 1985).

Otherwise unused grid points in the northwestern corner of the domain are connected to river entry points along the western edge of the domain. This arrangement allows approximately 100 km of the river channel to be simulated. In this way, most of the computer memory can be committed to solutions within the combined river-shelf domain. Similar techniques have been used in other applications of this model (Oey et al. 1985a; Galperin and Mellor 1990). The very strong tidal bore that occurs at the river mouth in nature is not specifically reproduced by the model. Instead, the river-channel grid points in the model damp the tidal bore as it moves upstream. This damping also occurs in nature, although the simplified river geometry in the model (a straight line of grid points) precludes direct comparison of the upstream tidal bore in the river with that in the model.

Model Boundary Conditions

A number of boundary conditions must be established in order to run a three-dimensional model like the one used here. For this study, surface wind stress is set equal to the climatological monthly values given by Hellerman and Rosenstein (1983). In many areas of the world, synoptic winds are much greater than climatological winds. Near the Equator, however, this effect is not as pronounced: synoptic winds are often very close to climatological averages (Tucker and Barry 1969). The net surface heat and salt flux is set to zero because the input of these variables to the surface of the modeling domain is minor compared to the influence of river heat and freshwater input. This approximation has been shown to be valid for most coastal areas of the equatorial Atlantic that are strongly influenced by the North Brazil Coastal Current (Flagg et al. 1986).

Tidal forcing in the model occurs only along the eastern edge of the domain. At the northern and southern edges the gradient of alongshore surface elevation, $\partial\eta/\partial y$, is zero. The four major tidal components—M_2 (principal lunar), S_2 (principal solar), K_1 (lunisolar diurnal), and O_1 (principal lunar diurnal)—were obtained from several sources. The amplitude of M_2 tidal forcing on the eastern border is 0.7 m, a value that approximately matches the tidal range along the 100-m isobath (Accad and Perkins 1978). Tides in the western equatorial Atlantic Ocean are dominantly M_2 (Defant 1961; Gibbs 1982). $S_2/(M_2 + S_2)$ is set at 0.3, a value that approximates published tidal records (Curtin and Legeckis 1986). Analysis of tidal components has shown that $(K_1 + O_1)/(M_2 + S_2) < 0.1$ in this part of the Atlantic (Defant 1961, his table 80). K_1 and O_1 were therefore set equal to zero.

Determination of mass flux into the southern part of the domain is problematic due to the paucity of three-dimensional current data in this part of the world. The seasonally averaged, historical ship-drift data of Richardson and McKee (1984) are used to specify mass flux at the southeastern corner of the domain. Vertically integrated mass flux is decreased proportionally in the shoreward direction until it is zero at the first land point. Mass flux in and out of the eastern boundary is determined by tidal elevations, with no net transport across this boundary. Mass flux in and out of the northern boundary is the sum of outflow from all other boundaries. River outflow is modeled as a seasonally varying sine wave with minimum flow (0.9 × 10⁵ m³/s) in mid-November and maximum flow (2.3 × 10⁵ m³/s) in mid-May. This closely parallels average observed river discharges (Oltman 1968).
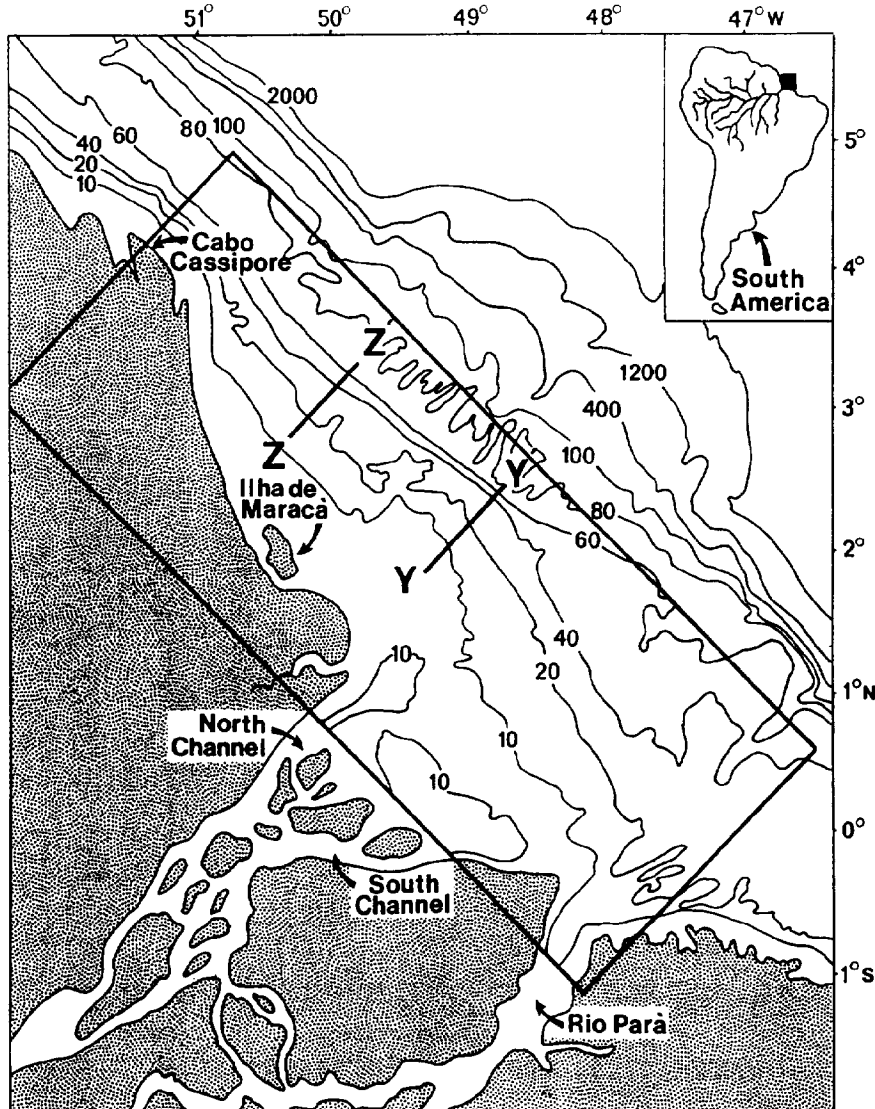
Fig. 1.—Location of the modeling domain on the continental shelf of northeastern Brazil. Contours represent depth in meters. Lines Y-Y' and Z-Z' mark the locations of cross-shelf property plots of Curtin (1986a).

Temperature and salinity boundary conditions along the southern, eastern, and northern boundaries of the model domain are taken from the data set of Levitus (1982) for flood-tide (inflow) conditions. During ebb tide (outflow), temperature and salinity were calculated using an "upwind" difference advection equation (Blumberg and Mellor 1987, their eq 23c). Amazon River temperatures are set at 28.5°C (Curtin 1986a) and river salinity is specified as 0 ppt.

Calculations of Bottom Shear Stress

Bottom shear stress is commonly determined from bottom velocities using a drag coefficient:

$$\tau_b = C_D \rho |V_b| V_b \tag{1}$$

where τ_b is the bottom shear stress, ρ is fluid density, V_b is the velocity of the bottom grid point, and C_D is the bottom drag coefficient. C_D is commonly calculated from a relationship based on the logarithmic law of the wall:

$$C_D = \left(\frac{1}{\kappa} \ln\left(\frac{z_b}{z_o}\right)\right)^{-2} \tag{2}$$

where κ is the von Kármán constant (0.4), z_b is height above the seafloor, and z_o is the effective sediment roughness length. The value of z_o, and therefore C_D, depends complexly on the sediment grain size, the geometry of the sediment bed, the bottom current velocity, and other factors.

Eqs (1) and (2) have been successfully applied to fluid flows in a wide variety of geophysical settings. Along continental shelves, however, the dynamic setting is complicated by the superposition of two kinds of currents: low-frequency geostrophic or tidal currents and high-frequency, oscillatory currents caused by surface waves. The low-frequency and high-frequency currents have boundary layers with thicknesses on the order of meters and tens of centimeters, respectively (Grant and Madsen 1986).

In recent years, oceanographers and sedimentologists have come to recognize that waves and currents interact in a complex, nonlinear way near the seafloor (Smith 1977; Grant and Madsen 1979). It is now clear that bottom shear stress caused by wave-current interactions is much greater than simply the sum of the bottom shear stress due to waves or
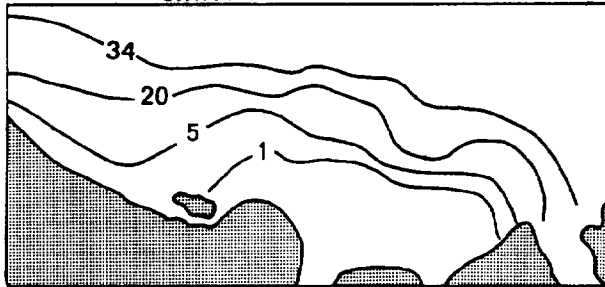
Gibbs
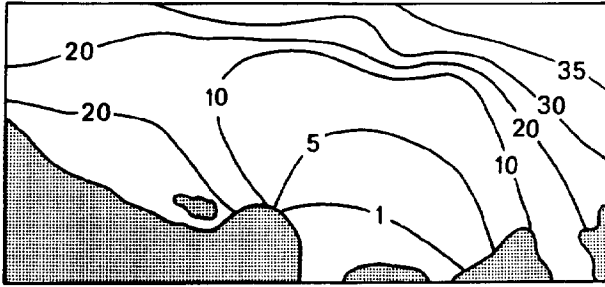
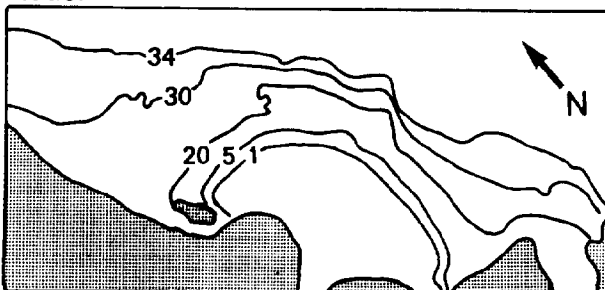**Szekielda**
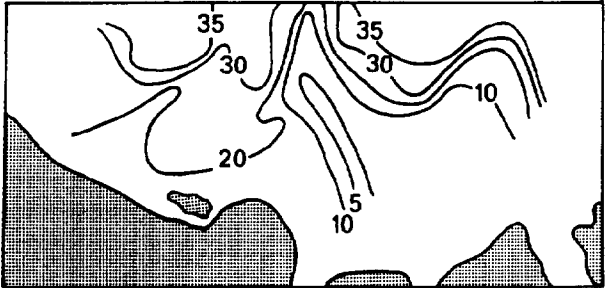
Gibbs and Konwar

Model

Fig. 2.—Diagrams of surface salinity (ppt) from Gibbs (1976), Szekielda et al. (1983), Gibbs and Konwar (1986), and the numerical model.

currents alone. Under certain conditions, the effective roughness length in Eq 2 can be increased by more than two orders of magnitude (Grant and Madsen 1979, their fig. 3). Since the Amazon dispersal system occupies a dynamic tidal régime in relatively shallow water (< 100 m), this phenomenon of combined wave-current bottom shear stress is probably very

important. Unfortunately, published procedures for calculating this effect are too cumbersome for a large-scale modeling project like the one described here. For instance, implementation of the theory of Grant and Madsen (1979) involves multiple integration of several functions as well as evaluation of a Kelvin function (a specialized Bessel function) for each seafloor location. Application of the complete version of this theory to the Amazon dispersal system would require these calculations to be made at nearly 2000 grid points at time steps equivalent to 15 minutes of real time. A simplified computational method that accounts for parts of the nonlinear wave-current theory was therefore developed for the sake of computational efficiency. It should be emphasized that this part of the project was meant to produce bottom shear-stress calculations that were an improvement over the simple "law of the wall" method, rather than accounting for all aspects of the relevant wave-current theories.

The initial step in applying this simplified wave-current calculation was to find wave orbital velocities from linear wave theory. Observations over the Amazon continental shelf (Meserve 1974) indicate average wave amplitudes of 0.5–1.0 m and wave periods of 6–7 s. During modeling runs, small wave amplitudes (0.5 m) were assumed near the coast and larger amplitudes (1.0 m) were assumed farther from the coast in deep water. For each grid point, the wave number k was calculated from the well known dispersion relation

$$\omega^2 = gk \tanh (kH) \qquad (3)$$

where ω is wave frequency, g is the acceleration of gravity, and H is depth. V_o can then be calculated from the equation

$$V_o = A_o \frac{2\pi\omega}{\sinh (kH)} \qquad (4)$$

where A_o is wave amplitude. Eq 4 yields very small orbital velocities (< 0.05 m/s) in water deeper than 30 m.

A general form for bottom shear stress that incorporates both current and wave orbital velocities (Grant and Madsen 1979, their eqs 19–20) is

$$|\tau_b| = \frac{1}{2}\rho f_{cw}\{|V_b|^2 + |V_o|^2 + |V_oV_b| \cos \alpha\} \qquad (5)$$

where α is the angle between the bottom current and the direction of wave propagation and f_{cw} is a friction factor that results from current and wave interaction. Eqs 1 and 5 have the same general form, indicating that a common expression can be derived that relates the drag coefficient C_D to the current-wave friction factor f_{cw}. Doing so in this study was desirable because the drag coefficient C_D was imbedded in existing computer code.

Equating the expressions for C_D and f_{cw} involved several simplifications and assumptions. First, model velocity output was taken to represent the current velocity V_b in Eq 5. In reality, the model output represented the combined effects of current and waves in those parts of the domain where this method was applied. A second simplification involved deriving an algebraic expression for f_{cw} from graphs in Grant and Madsen (1979). Use of the algebraic expression matched the Grant and Madsen results within 20% (Jewell 1989). Furthermore, the wave-current calculations were made only where the current velocity was less than twice the wave velocity. In deep water (> 30 m), where wave velocities were low, calculations were made with Eq 2. At each time step, all drag coefficients were spatially averaged with adjacent nodes in order to mitigate the effects of going between law-of-the-wall and wave-current formulations. Finally it should be noted that C_D is dependent on depth, whereas f_{cw} is a generalized expression for mean flow on the continental shelf. The wave-current shear stress equation was generally applied to water depths of 10–25 m. Within this depth range, C_D varies by a factor of 2 (Eq 2). This variation is not accounted for in Eq 5. However, this twofold variation is small when
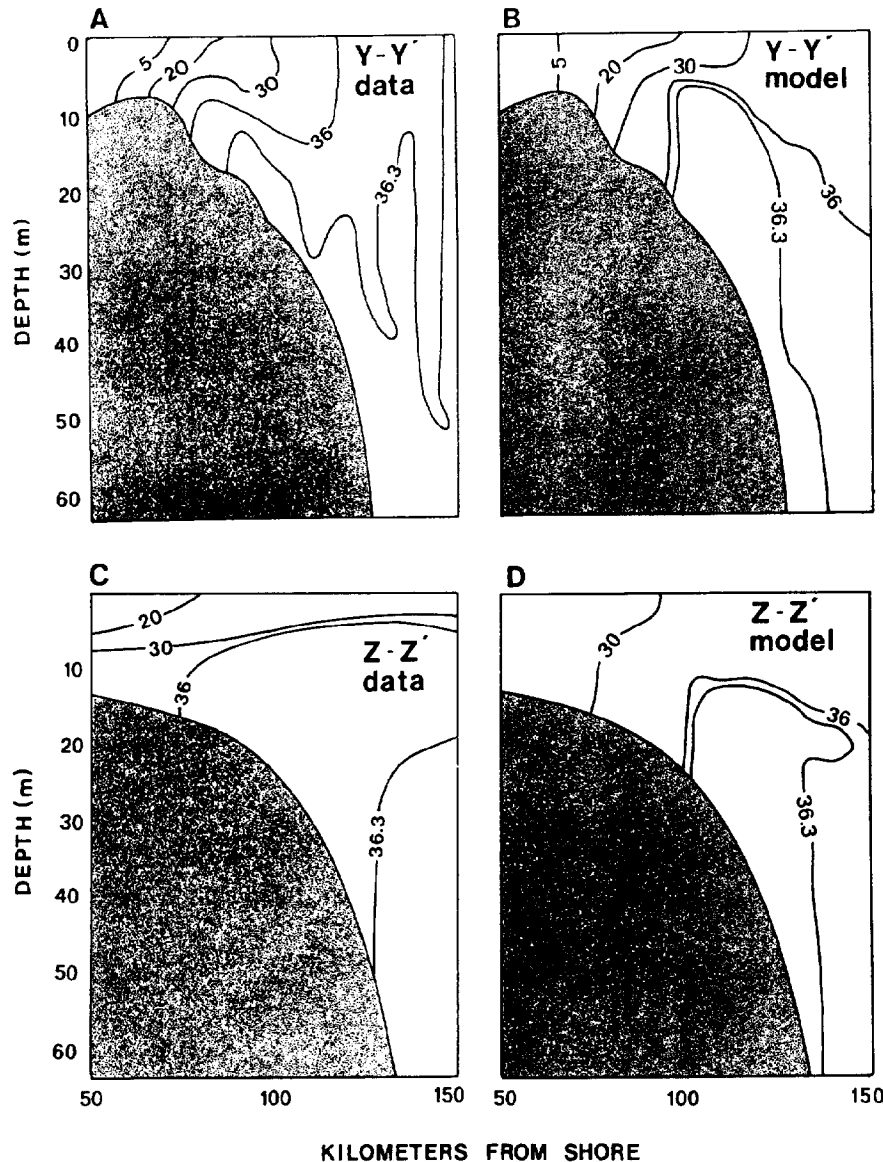
Fig. 3.—Cross-shelf transects of salinity (ppt). A) Salinity data at section Y-Y' of Figure 1 (Curtin 1986a). B) Model salinity at Section Y-Y' of Figure 1. C) Salinity data at Section Z-Z' of Figure 1 (Curtin 1986a). D) Model salinity of section Z-Z' of Figure 1.

compared to variability in f_{cw} caused by the ratio V_b/V_o and α (Grant and Madsen 1979, their fig. 4).

The results of this method of calculating bottom shear stress were effective, if not theoretically satisfying. Enhanced shear stress was shown to exist in intermediate-depth water (10–30 m), where the effect of combined wave-current interaction should be the most important. Drag coefficients varied significantly over tidal cycles, as would be expected in a dynamic regime where currents are extremely variable. Finally, it should be noted that simulations run using only the law of the wall showed greater vertical salinity stratification than either field data or model runs with the wave-current shear-stress formulation presented here.

MODEL RESULTS

Model simulations for an entire year were made in order to establish baselines for distributions of temperature and salinity as a function of seasonal river discharge onto the shelf. Output corresponding to the first day of each month was saved. In this way, additional model simulations could be restarted at any point during the year to study changes in model forcing parameters (i.e., winds, tides, and river discharge). Unless otherwise stated, the results given below represent model simulations during a month of high river discharge (May). Climatological average values of surface wind stress and river discharge were used in all model runs. Although synoptic forcings would give more realistic output, the present study is intended to show how model output compares to field data and to highlight seasonal variations in bottom shear stress. In all model results, cross-shelf refers to the northeast-southwest direction (Fig. 1) and long-shore refers to the northwest-southeast direction.

Model Validation

Validation of the model output is a problem because the domain covers thousands of square kilometers and flows vary on very short time scales. Under these conditions, it is difficult to obtain consistent and comprehensive data bases for any variable. Velocity data are sparse (Gibbs 1982; Curtin 1986b). Temperature is not particularly good for model diagnostics
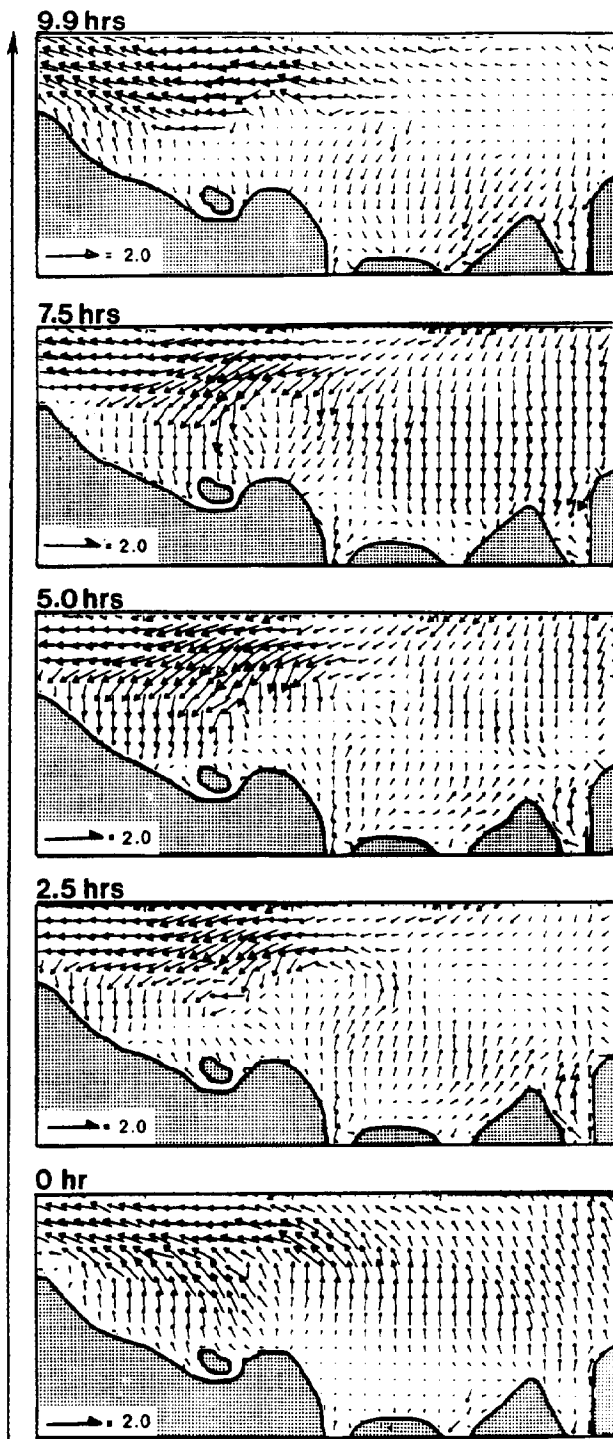
Fig. 4.—Simulated surface velocity over an M_2 tidal cycle (12.42 hours). Each frame represents a change of approximately 2.5 hours. The next 2.5 hour step after the last frame would be the same as the first frame. Scale bars are in meters/second.
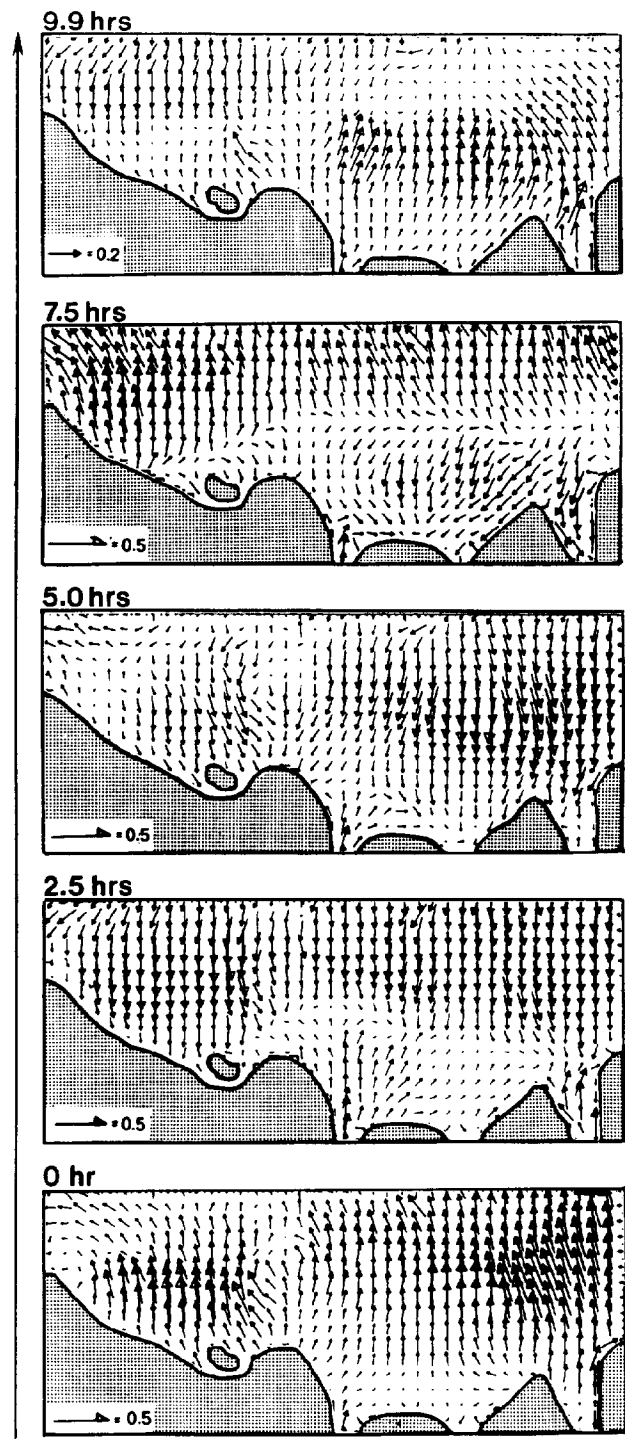

Fig. 5.—Simulated bottom velocity over an M_2 tidal cycle (12.42 hours). Each frame represents a change of approximately 2.5 hours. The next 2.5 hour step after the last frame would be the same as the first frame. Scale bars are in meters/second.

because the maximum temperature contrast between river and ocean water is only 2°C (Gibbs 1976; Curtin 1986b). Salinity is probably the best variable for model diagnostics because the contrast between river and ocean salinities is very large (0–36.5 ppt) and several data bases are available.

Salinity

Various surface-salinity data sets for similar conditions of river discharge appear to be inconsistent with one another (Fig. 2). Certain features of the model output and the surface-salinity data sets are consistent, how-

ever. Both data and model output show large horizontal gradients of cross-shelf surface salinity (approximately 1 ppt/km). Alongshore salinity gradients in both model simulations and data are more than an order of magnitude smaller. The model predicts surface salinity very well near the river mouth. In the northern part of the domain, the model surface salinity compares well with the salinity data plots of Gibbs and Konwar (1986) and Szekielda et al. (1983). Surface salinity in the northern part of the model area is 10–15 ppt greater than the data of Gibbs (1976). In shallow water, simulated surface salinity is much greater than the data of Gibbs and Konwar (1986). It should be noted, however, that coverage of field data on salinity in shallow water is sparse, particularly north of the river mouth.

Cross-shelf salinity transects provide a more consistent check on the validity of model results than does surface salinity because these transects often are completed in days rather than weeks. Two salinity transects from the 1983 R/V Iselin cruise are shown in Figure 3. Several features of the simulated salinity transect near the river mouth (Section Y–Y', Fig. 1) compare well with the data of Curtin (1986a) (Fig. 3A, B). The water column is well mixed at depths less than 7 m in both the salinity data and the salinity model simulations. The characteristic salt wedge is developed in water deeper than 10 m and extends 120 km offshore. Upward bowing of the 36-ppt and 36.3-ppt isohalines is evident at 5–10 m depths in the salt wedge. Curtin (1986a) attributes this feature to the strong freshwater outflow, which causes upwelling of underlying salt water.

The simulated cross-shelf salinity in shallow water along a transect in the northern part of the plume (Section Z–Z' in Fig. 1) is much higher than the salinity data of Curtin (1986a). In deeper water, the basic features of the salt wedge and deep isohaline structure (salinity > 36 ppt) of the data set is well reproduced by the simulations.

Differences between model simulations and field observations of salinity probably arise from several sources. Inflow boundary conditions are only approximate because they are extrapolated from a coarse-resolution data set (Levitus 1982; Richardson and McKee 1984). The horizontal grid spacing of the model is sufficiently coarse (7.8 km) that subgrid turbulence is not completely resolved. As mentioned previously, wind forcing in the simulations relies on climatological averages rather than synoptic data.

Velocity and Shear Stress Over a Tidal Cycle

Calculated surface velocity over a tidal cycle shows the dominance of the North Brazil Coastal Current in the northern portion of the offshore portion of the Amazon continental shelf (Fig. 4). Onshore-offshore tidal flow is dominant in the shallow water, closer to shore. Tidal flow tends to overwhelm the river plume in much of the surface domain (Fig. 4).

Water circulation and bottom shear stress exhibit complex spatial and temporal variability. The influence of river outflow can be seen near the river mouth, although the magnitudes of river velocities are small relative to tidal velocities (Fig. 5). Tidal currents in the northern and southern parts of the model domain are very strong: over a tidal cycle, bottom-current speeds vary by as much as 1 m/s. Bottom shear stress plotted over an M_2 (principal lunar) tidal cycle follows the general pattern of bottom currents (Fig. 6) and shows considerable spatial variability. Local zones of high shear stress (> 5 dynes/cm^2) are present near the river month and immediately to the north at various points in the tidal cycle. In shallow water, bottom shear stress can vary by more than an order of magnitude over periods as short as 2–3 hours. At intermediate depths (20–40 m) bottom shear stress is on the order of 1–5 dynes/cm^2. Seaward of the 40-m isobath bottom shear stress is 0.2–2 dynes/cm^2 and remains relatively constant over a tidal cycle.

MODEL OUTPUT AND OBSERVED SEDIMENT FEATURES

The present status of sediment-transport theory and numerical modeling as well as the lack of comprehensive field observations in the large Amazon
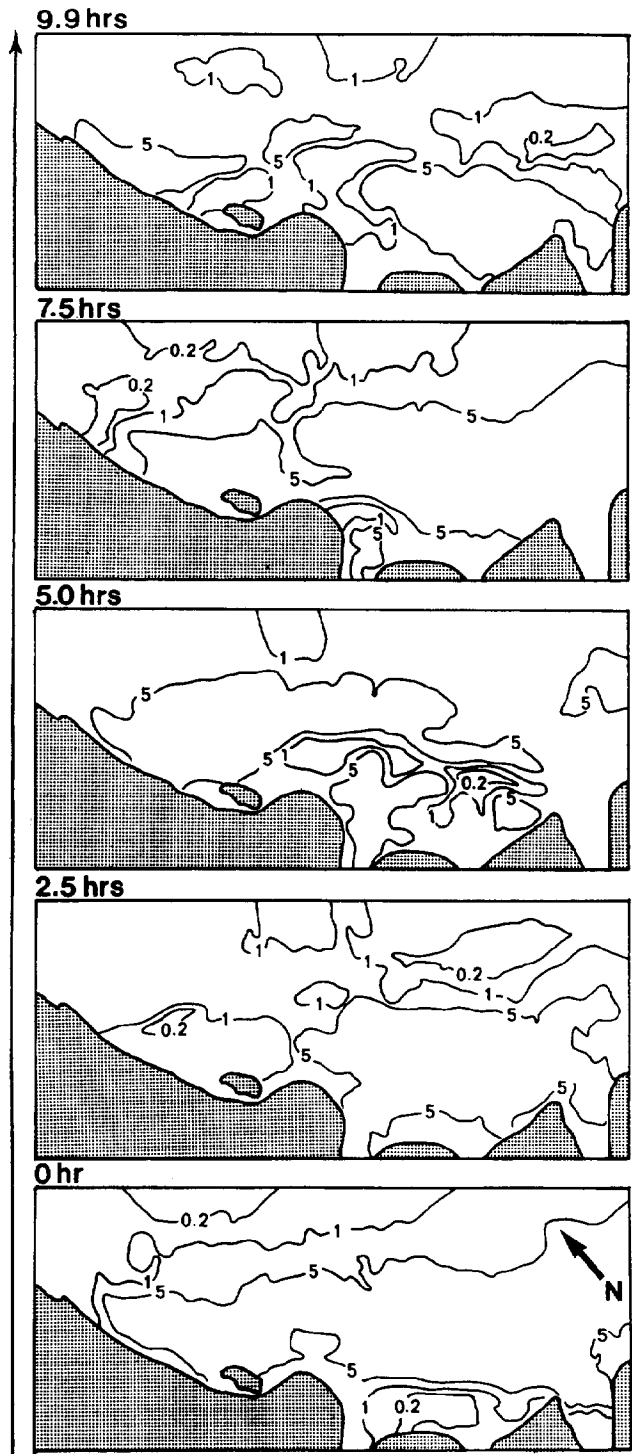

Fig. 6.—Simulated distribution of bottom shear stress (dynes/cm^2) over an M_2 tidal cycle. The frames in Figure 6 correspond in time to those in Figures 4 and 5.

dispersal system make quantitative predictions of sediment transport difficult. This is particularly true on the Amazon continental shelf, where there are powerful tidal currents, a strong, through-flowing western boundary current, and waves that interact nonlinearly with both kinds of cur-
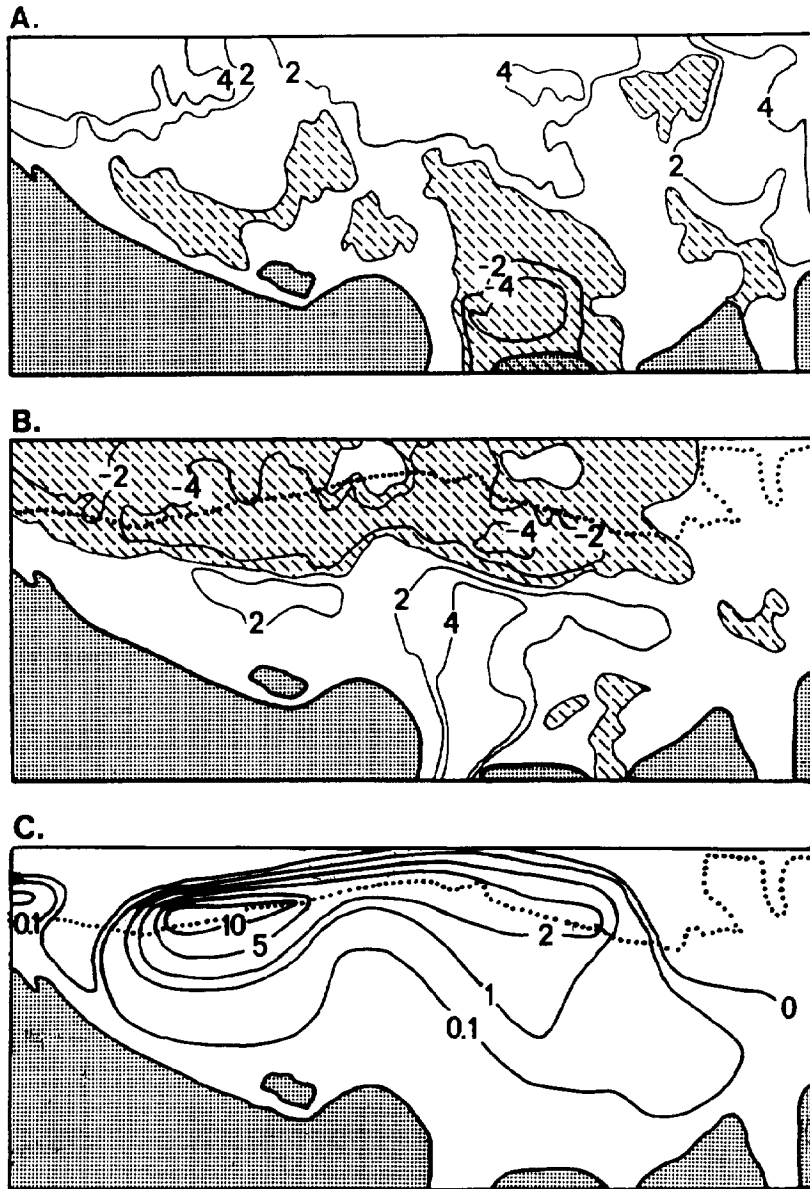
A.

B.

C.

Fig. 7.—A) Longshore component of residual tidal velocity (cm/s). Positive values are in the northwest direction (toward the left of the figure). B) Onshore-offshore component of residual tidal velocity (cm/s). Positive values are in northeast direction (toward the top of the figure). C) Sediment accumulation rates in the estuary in cm/yr (from Kuehl et al. 1986). Dotted line is the 40-m isobath.

rents. These factors combine to create a complex pattern of sediment dispersal and deposition. Nevertheless, our state-of-the-art model can be used in conjunction with known features of the Amazon continental shelf to make general observations about the most important physical processes influencing sedimentation. Three specific results of the numerical model are examined within the context of observed sediment features: residual tidal velocities, the maximum observed bottom shear stress over a tidal cycle, and the seasonal difference in maximum bottom shear stress.

Residual Tidal Velocities and Sediment Accumulation

Computing the residual tidal velocity is one way to determine net water transport over a tidal cycle. Residual tidal velocity is defined as

$$\bar{U} = \frac{1}{T} \int_0^T U \, dt \tag{6}$$

where T is the tidal period (in this case the M_2 tide). Computed residual tidal velocities near the sea floor can be examined to see if there is any correspondence between net water transport and net sediment transport rate.

On the Amazon continental shelf, net longshore flow is to the north along the outer part of the shelf whereas longshore circulation patterns are more complex in shallow water (Fig. 7A). Residual offshore tidal velocities are high near the mouth of the Amazon River (Fig. 7B). Onshore-offshore residual tidal velocities reverse sign in intermediate-depth water north of the Amazon River mouth. This reversal of sign lies shoreward of the zone of maximum sediment accumulation (Fig. 7C). The area of rapid sediment accumulation corresponds to the prograding, subaqueous delta described by Nittrouer et al. (1986) and is close to the 40-m isobath.

A possible explanation for the area of rapid sediment accumulation can be seen in plots of onshore-offshore residual tidal velocity at several depths in the water column (Fig. 8). Significant offshore water transport adjacent to the river mouth exists at all vertical levels of the model. For this reason,

high concentrations of river-borne suspended sediment are swept offshore over the continental shelf and then northward by the North Brazil Coastal Current. As the sediment settles through the water column, it is subjected to the net onshore residual velocities near the bottom (Figs. 7B, 8). The result is rapid sediment accumulation immediately shoreward of the 40-m isobath.

Maximum Bottom Shear Stress Over a Tidal Cycle

Maximum bottom shear stress (Fig. 9A) is defined as the maximum root-mean-square sum of the two shear components over an M_2 tidal cycle (12.42 hours). The maximum bottom shear stress occurs at different times for different model grid points, so the plot in Figure 9A represents a scalar quantity (magnitude of the shear stress) that does not have a directional property.

Maximum simulated bottom shear stress over an M_2 tidal cycle (Fig. 9A) shows patterns that correspond closely to sediment deposition rates (Fig. 9B). There is an area of shallow water (< 20 m depth) and exceptionally high maximum shear stress (> 25 dynes/cm^2) near the river mouth and Ilha de Maraca. This is also an area where sediment accumulation rates are extremely low (Fig. 7B). Sediment accumulation rates are on the order of 0.1 cm/yr where simulated maximum bottom shear stress is greater than 10 dynes/cm^2. Sediment accumulation rates are observed to be greatest near the seaward edge of the model domain, where the maximum bottom shear stress is approximately 5 dynes/cm^2 and corresponds roughly to the 40-m isobath (Fig. 9B). As mentioned previously, the general increase in sediment accumulation rate from south to north along the 40-m isobath is due to northward movement of suspended sediment in the Amazon plume rather than a north-to-south change in bottom shear stress. It is interesting to note that a subtle change in sediment accumulation at the very northern part of the model domain coincides with the general contours of computed bottom shear stress.

Sediment Transport Mechanics

Amazon River water that discharges over the continental shelf has very high concentrations (> 200 mg/kg) of suspended sediment. The suspended sediment settles out of the water column as the Amazon plume is swept northward by the North Brazil Coastal Current (Fig. 4). Sedimentation rates are enhanced by the interaction of the freshwater river plume with seawater because the high ionic strength of seawater increases floc diameter of suspended sediment approximately tenfold (Gibbs and Konwar 1986).

Observed features of Amazon sedimentation can be described qualitatively with the aid of the sediment continuity equation (e.g., Middleton and Southard 1983, their eq 7-23):

$$\frac{\partial h}{\partial t} = -K_1 \left(\frac{\partial q_x}{\partial x} + \frac{\partial q_y}{\partial y} + H \frac{\partial C}{\partial t} \right) \tag{7}$$

where h is height of the sediment-water interface above some reference level, H is water depth, q_x and q_y are horizontal sediment transport rates, C is suspended sediment concentration, and K_1 is a dimensionless constant. Sediment transport rate q is the depth-integrated product of local suspended sediment concentration and the local time-average velocity.

If sedimentation is considered on time scales much greater than a tidal cycle, then sedimentation is essentially steady state, i.e., the transient term in the sediment continuity equation, $\partial C/\partial t$, is zero. Since $\partial h/\partial t$ is also nonzero (i.e., sediment is being deposited) (Fig. 9A), the divergence of the horizontal sediment transport q (representing the product of velocity and sediment concentration), must also be nonzero. Plots of the residual tidal velocity field (Fig. 7) show that the zones of greatest gradients of residual tidal velocity do not correspond very well with areas of rapid sediment accumulation. Instead, the $\partial q_x/\partial x$ and $\partial q_y/\partial y$ terms are nonzero where
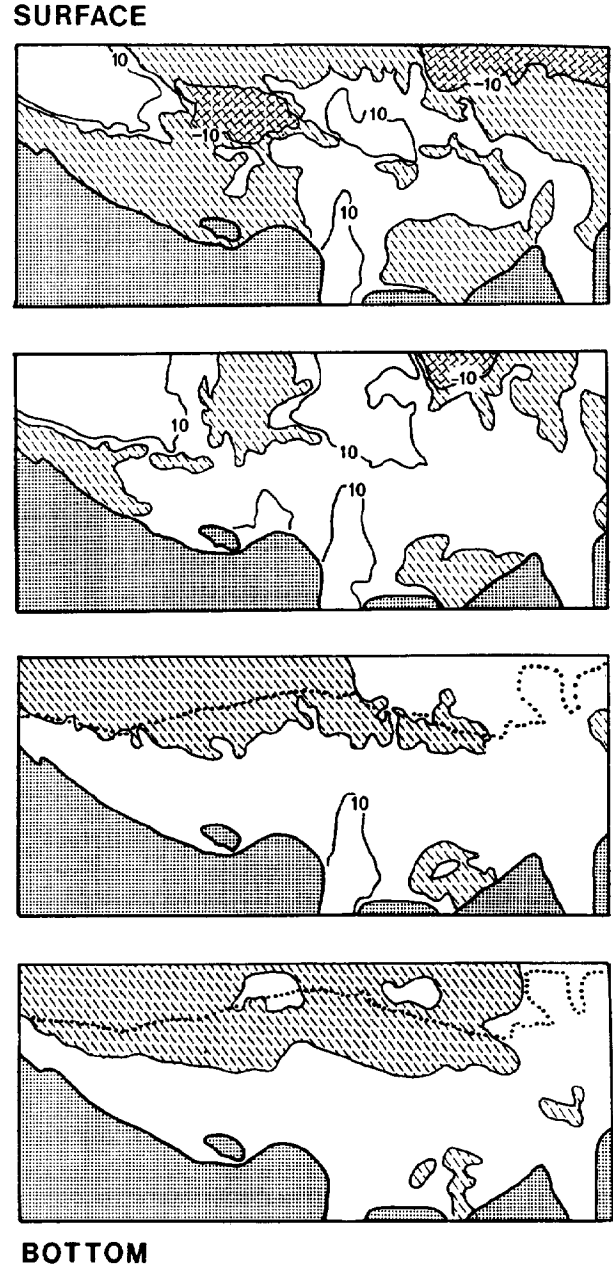
FIG. 8.—Onshore-offshore component of residual tidal velocity (cm/sec) plotted at various model levels. Dashed pattern in the estuary represents onshore velocity, and white areas represent offshore velocity. Dotted lines represent the 40-m isobath.

the concentration gradients are also nonzero. These concentration gradients become significant for two reasons. First, sediment is being removed from the water column due to flocculation along time-averaged streamlines of the Amazon plume as it is advected along the continental shelf by the North Brazil Coastal Current. Gradients of suspended sediment concentration along these streamlines are therefore nonzero. Sediment-concentration gradients are also appreciable where offshore-flowing sediment-bearing water encounters onshore-flowing sediment-barren water (Figs. 7, 8). The spatial terms on the right side of Eq 7 is thus nonzero, and sediment accumulation is focused at intermediate depths of the continental shelf.

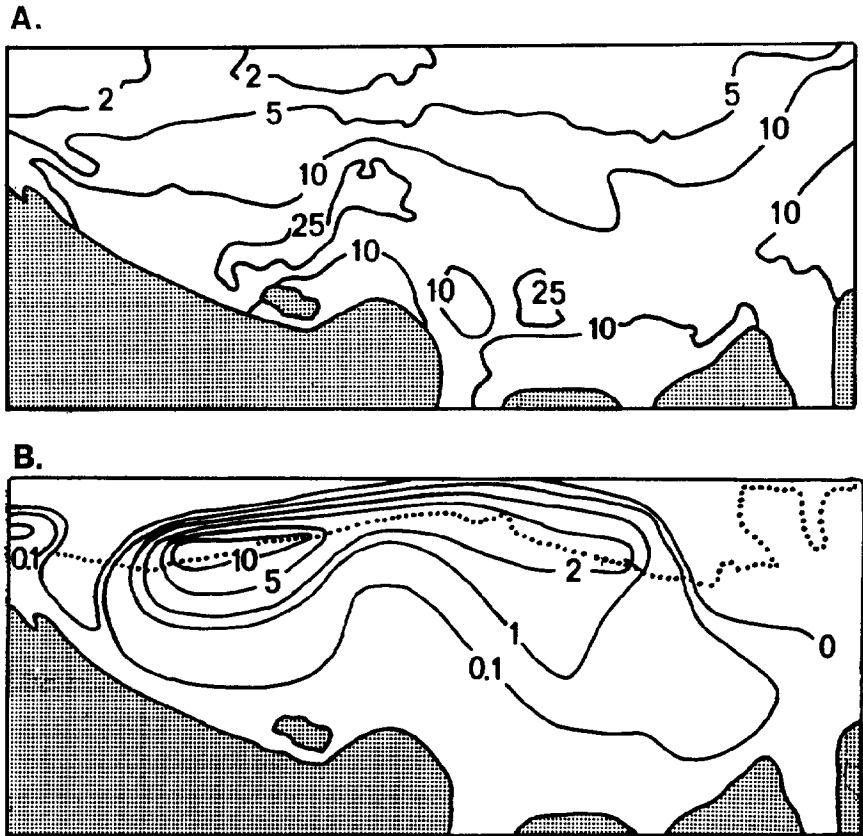Further insight into patterns of sediment deposition can be gained by

A.

B.

Fig. 9.—A) Simulated maximum bottom shear stress (dynes/cm²) over an M_2 tidal cycle at high river discharge. B) Sediment accumulation rates in the estuary in cm/yr (from Kuehl et al. 1986). Dotted line is the 40-m isobath.

considering the maximum shear stress over a tidal cycle. For noncohesive sediment, equations for sediment transport rate can have several possible forms (e.g., Allen 1984; Sleath 1984). A typical expression (Allen 1984, his eq. 2-30) is

$$q = \frac{K_2}{(\rho_s - \rho_w)g}(\tau - \tau_{cr})^m \tag{8}$$

where ρ_s and ρ_w are the density of sediment and water, respectively, τ is bottom shear stress, and K_2 is an empirically determined coefficient whose dimensions depend on variables used in the equations and values of the exponent m. The subscript cr refers to the shear stress necessary to initiate sediment motion. If the maximum shear stress observed in a tidal cycle exceeds the critical shear stress needed to initiate sediment motion (Eq. 8) and the divergence of the sediment transport rate is small (Eq 7), then there is no sediment deposition. This is clearly the case in the shallow parts of the Amazon continental shelf (Figs. 7, 9).

Seasonal Differences in Bottom Shear Stress

The model simulations indicate that substantial variations in bottom shear stress exist in the Amazon Estuary between high and low river discharge (Fig. 10A). River discharge follows a seasonal pattern, with high river flow in May–June (approximately 225,000 m³/s) and low discharge in October–November (approximately (90,000 m³/s) (Oltman 1968). Although the overall model pattern is irregular, seasonal differences (as much as 5 dynes/cm²) are present north and seaward of the river mouth. Interestingly, sediment lithologies in this area consist of interbedded mud and sand, indicating a time-varying depositional regime for this part of the

estuary (Fig. 10B; Kuehl et al. 1982). South of the river mouth and north of Ilha De Maraca, sediments are faintly laminated muds. Model output for these regions indicates that seasonal variations in bottom shear stress are approximately 1 dyne/cm². In deeper water, seasonal shear-stress distributions are less than 1 dyne/cm², and sediment lithology consists of bioturbated mud. The combination of bottom shear stress simulations and sediment observations therefore indicates that the laminated sediments are the result of seasonal differences in distribution of bottom shear stress. It is not yet possible to determine whether these seasonal differences are caused by changes in river discharge (from 90,000 m³/s to 225,000 m³/s) or changing seasonal wind shear stress. The general progression of high seasonal shear-stress differences near the river mouth to low seasonal differences along the shelf margin indicates that river discharge is the more important factor.

DISCUSSION

This study presents a three-dimensional circulation model coupled to a combined wave-current interaction model of bottom shear stress. The combined model is used to address sediment transport dynamics as well as observed sedimentology of the Amazon continental shelf. Sediment accumulation rates on the Amazon shelf appear to be controlled by three factors: (1) unloading of suspended sediment as the Amazon plume is swept northward by the North Brazil coastal current; (2) large magnitude and (in a time-average sense) crude uniformity of bottom shear stress over a tidal cycle in the shallow parts of the shelf, resulting in no sediment accumulation, and (3) the convergence of onshore-flowing sediment-barren water and offshore-flowing sediment-bearing water masses at intermediate depths of the continental shelf. The result is the prograding, subaqueous delta described by Nittrouer et al. (1986). Model results suggest

A.

bioturbated
mud

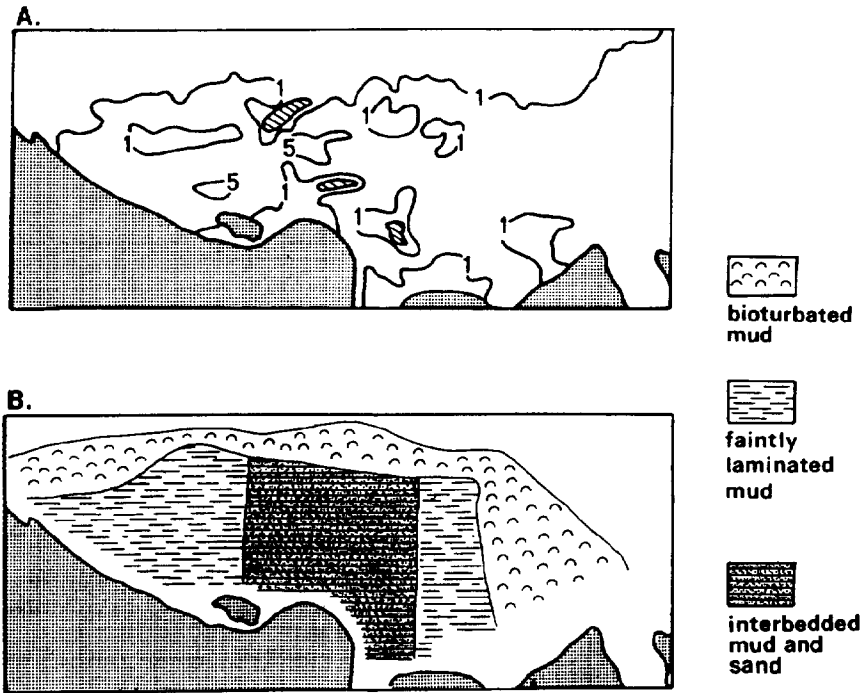**B.**

faintly
laminated
mud

interbedded
mud and
sand

FIG. 10.—A) Differences in maximum bottom shear stress between high river discharge and low river discharge in dynes/cm². Lined pattern indicates that shear stress at low river discharge is higher than at high river discharge. B) Distribution of bottom sediment type in the Amazon estuary (from Kuehl et al. 1982).

that continued growth of the delta is to be expected at the northern edge of the present delta, in intermediate-depth water, rather than seaward in deep water.

Kuehl et al. (1982) have suggested that short-term increases of Amazon River discharge are responsible for deposition of the sand component of the interlaminated sediments outside the river mouth. Our model used a smoothly varying, sinusoidal river input. Model results suggest that changes from high to low river discharge cause significant differences in bottom shear stress (Fig. 10). A similar effect might be expected for short-term flooding episodes like those envisioned by Kuehl et al. (1982).

Models like ours have the potential to aid in the study of ancient sedimentary environments. One possible future application of the model might be to predict sediment accumulation on continental shelves during transgressive and regressive cycles. For instance, by taking oceanographic and atmospheric boundary conditions from studies of Pleistocene climate, it might be possible to reconstruct various depositional regimes of the Amazon delta during the past 12,000 years. Similar work has been attempted in the well studied Cretaceous Interior Seaway of North America (Eriksen and Slingerland 1990) with a nonstratified model that uses a Chézy-Manning method for bottom shear stress. A more sophisticated model like ours might elucidate the relative influence of tides, river discharge, and wind-induced wave motions. We emphasize, however, that computational studies of ancient environments can only approximate actual sediment dynamics. Such work is often most useful in making sensitivity analyses of the relevant physical variables.

ACKNOWLEDGMENTS

REFERENCES

ACCAD, Y., AND PERKINS, C.L., 1978, Solution of tidal equation for M₂ and S₂ tides in the world ocean from a knowledge of the tidal potential alone: Royal Society (London) Philosophical Transactions, Series A, v. 290, p. 235–266.

ALLEN, J.R.L., 1984, Sedimentary Structures: Their Character and Physical Basis: Amsterdam, Elsevier, 663 p.

ALLER, J.Y., AND ALLER, R.C., 1986, General characteristics of benthic faunas on the Amazon inner continental shelf with comparison to the shelf off the Changjiang River, East China Sea: Continental Shelf Research, v. 6, p. 291–310.

BLUMBERG, A.F., AND MELLOR, G.L., 1987, A description of a three-dimensional coastal ocean circulation model, in Heaps, N.S., ed., Three Dimensional Coastal Ocean Models: American Geophysical Union, Coastal and Estuarine Science, v. 4, p. 1–16.

BOWLES, F.A., AND FLEISCHER, P., 1985, Orinoco and Amazon River sediment input to the eastern Caribbean basin: Marine Geology, v. 68, p. 53–72.

CURTIN, T.B., 1986a, Physical observations in the plume region of the Amazon River during peak discharge—II. Water masses: Continental Shelf Research, v. 6, p. 53–71.

CURTIN, T.B., 1986b, Physical observations in the plume region of the Amazon River during peak discharge—III. Currents: Continental Shelf Research, v. 6, p. 73–86.

CURTIN, T.B., AND LEGECKIS, R.V., 1986, Physical observations in the plume region of the Amazon River during peak discharge—I. Surface variability: Continental Shelf Research, v. 6, p. 31–51.

DAMUTH, J.E., 1977, Late Quaternary sedimentation in the western equatorial Atlantic: Geological Society of America Bulletin, v. 88, p. 695–710.

DAMUTH, J.E., AND KUMAR, N., 1975, Amazon cone—morphology, sediments, age, and growth pattern: Geological Society of America Bulletin, v. 86, p. 863–878.

DAVIES, A.G., SOULSBY, R.L., AND KING, H.L., 1988, A numerical model of the combined wave and current bottom boundary layer: Journal of Geophysical Research, v. 93, p. 491–508.

DEFANT, A., 1961, Physical Oceanography, Vol. II: New York, Pergamon Press, 590 p.

DeMASTER, D.J., KUEHL, S.A., AND NITTROUER, C.A., 1986, Effects of suspended sediments on geochemical processes near the mouth of the Amazon River—examination of biological silica uptake and the fate of particle-reactive elements: Continental Shelf Research, v. 6, p. 107–125.

DRAKE, D.E., AND CACCHIONE, D.A., 1986, Field observations of bed shear stress and sediment resuspension on continental shelves: Continental Shelf Research, v. 6, p. 415–429.

DYER, K.R., 1986, Coastal and Estuarine Sediment Dynamics: Wiley-Interscience, New York, 342 p.

EDMOND, J.M., BOYLE, E.A., GRANT, B., AND STALLARD, R.F., 1981, The chemical mass balance in the Amazon plume—I. The nutrients: Deep Sea Research, v. 28, p. 1339–1374.

ERIKSEN, M.C., AND SLINGERLAND, R.L., 1990, Numerical simulations of tidal and wind-driven circulation in the Cretaceous Interior Seaway of North America: Geological Society of America Bulletin, v. 102, p. 1499–1516.

FLAGG, C.N., GORDON, R.L., AND McDOWELL, S., 1986, Hydrographic and current observations on the continental slope and shelf of the western equatorial Atlantic: Journal of Physical Oceanography, v. 16, p. 1412–1429.

GALPERIN, B., AND MELLOR, G.L., 1990, A time-dependent, three-dimensional model of the Delaware Bay and River system. Part 1: Description of the model and tidal analysis: Estuarine, Coastal, and Shelf Science, v. 31, p. 231–253.

GIBBS, R.J., 1967, The geochemistry of the Amazon River system: part I. The factors that control the salinity and the composition and concentration of the suspended solids: Geological Society of America Bulletin, v. 78, p. 1203–1232.

GIBBS, R.J., 1976, Amazon River sediment transport in the Atlantic Ocean: Geology, v. 4, p. 45.

GIBBS, R.J., 1982, Currents on the shelf of northeastern South America: Estuarine, Coastal, and Shelf Science, v. 14, p. 283–299.

GIBBS, R.J., AND KONWAR, L., 1986, Coagulation and settling of Amazon River suspended sediment: Continental Shelf Research , v. 6, p. 127–149.

GRABER, H.C., BEARDSLEY, R.C., AND GRANT, W.D., 1989, Storm generated surface waves and sediment resuspension in the East China and Yellow Seas: Journal of Physical Oceanography, v. 19, 1039–1059.

GRANT, W.D., AND MADSEN, O.S., 1979, Combined wave and current interaction with a rough bottom: Journal of Geophysical Research, v. 84, p. 1797–1807.

GRANT, W.D., AND MADSEN, O.S., 1986, The continental shelf bottom boundary layer: Annual Review of Fluid Mechanics, v. 18, p. 265–305.

GRANT, W.D., WILLIAMS, A.J., AND GLENN, S.M., 1984, Bottom stress estimates and their prediction on the northern California continental shelf during CODE-1: the importance of wave-current interaction: Journal of Physical Oceanography, v. 14, p. 506–527.

HELLERMAN, S., AND ROSENSTEIN, M., 1983, Normal monthly wind stress over the world ocean with error estimates: Journal of Physical Oceanography, v. 13, p. 1093–1104.

JEWELL, P.W., 1989, Fluid dynamic and geochemical models of shallow lakes, the Amazon estuary, and bedded barite deposits [unpublished Ph.D. thesis]: Princeton University, Princeton, New Jersey, 200 p.

KEY, R.M., STALLARD, R.F., MOORE, W.S., AND SARMIENTO, L., 1985, Distribution and flux of Ra-226 and Ra-228 in the Amazon estuary: Journal of Geophysical Research, v. 90, p. 6995–7004.

KROOK, L., 1979, Sediment petrographical studies in northern Suriname [unpublished Ph.D. thesis]: University of Amsterdam, 154 pp.

KUEHL, S.A., DEMASTER, D.J., AND NITTROUER, C.A., 1986, Nature of sediment accumulation on the Amazon continental shelf: Continental Shelf Research, v. 6, p. 209–225.

KUEHL, S.A., NITTROUER, C.A., AND DEMASTER, D.J., 1982, Modern sediment accumulation and strata formation on the Amazon continental shelf: Marine Geology, v. 49, p. 279–300.

LEVITUS, S., 1982, Climatological atlas of the world ocean: National Oceanic and Atmospheric Administration Professional Paper 13, United States Government Printing Office, Washington, D.C., 173 p.

MELLOR, G.L., AND KANTHA, L., 1989, An ice-ocean model: Journal of Geophysical Research, v. 94, p. 10,937–10,954.

MELLOR, G.L., AND YAMADA, T., 1982, Development of turbulence closure models for geophysical fluid dynamics problems: Reviews of Geophysics and Space Physics, v. 20, p. 851–875.

MESERVE, J.M., 1974, U.S. Navy marine climatic atlas of the world, Vol. 1, North Atlantic Ocean: United States Government Printing Office, Washington D.C., 371 p.

MIDDLETON, G.V., AND SOUTHARD, J.B., 1984, Mechanics of Sediment Transport: SEPM Short Course 3, 401 p.

MILLIMAN, J.D., AND MEADE, R.H., 1983, World-wide delivery of river sediment to the oceans: Journal of Geology, v. 91, p. 1–21.

MILLIMAN, J.D., SUMMERHAYES, C.P., AND BARRETTO, H.T., 1975a, Oceanography and suspended matter off the Amazon River, February–March, 1973: Journal of Sedimentary Petrology, v. 45, p. 189–206.

MILLIMAN, J.D., SUMMERHAYES, C.P., AND BARRETTO, H.T., 1975b, Quaternary sedimentation on the Amazon continental margin—a model: Geological Society of America Bulletin, v. 86, p. 610–614.

NELSON, B.W., ed., 1972, Environmental Framework of Coastal Plain Estuaries: Geological Society of America Memoir 133, 619 p.

NITTROUER, C.A., KUEHL, S.A., DEMASTER, D.J., AND KOWSMANN, R.O., 1986, The deltaic nature of Amazon sedimentation: Geological Society of America Bulletin, v. 97, p. 444–458.

OEY, L.-Y., MELLOR, G.L., AND HIRES, R.I., 1985a, Tidal modeling of the Hudson-Raritan estuary: Estuarine, Coastal, and Shelf Science: v. 20, p. 511–527.

OEY, L.-Y., MELLOR, G.L., AND HIRES, R.I., 1985b, A three-dimensional simulation of the Hudson-Raritan estuary. Part I. Description of the model and model simulations: Journal of Physical Oceanography, v. 15, p. 1676–1692.

OLTMAN, R.E., 1968, Reconnaissance investigations of river discharge and water quality of the Amazon River: United States Geological Survey Circular 552, Washington, D.C., 16 p.

RICHARDSON, P.L., AND McKEE, J.K., 1984, Average seasonal variation of the Atlantic North Equatorial Countercurrent from ship drift data: Journal of Physical Oceanography, v. 14, p. 1226–1238.

SHENG, Y.P., AND LICK, W., 1979, The transport and resuspension of sediments in a shallow lake: Journal of Geophysical Research, v. 84, p. 1809–1826.

SHOLKOVITZ, E.R., AND PRICE, N.B., 1980, The major-element chemistry of suspended matter in the Amazon estuary: Geochimica et Cosmochimica Acta, v. 44, p. 163–171.

SLEATH, J.F.A., 1984, Sea Bed Mechanics: New York, Wiley-Interscience, 335 p.

SMITH, J.D., 1977, Modeling of sediment transport on continental shelves, in Goldberg, E.T., McCave, I.N., O'Brien, J.J., and Steele, J.H., eds., The Sea, Vol. 6, New York, Wiley-Interscience, p. 539–577.

SZEKIELDA, H.-K., McGINNIS, D., AND GIRO, R., 1983, Investigations with satellites on eutrophication of coastal regions, in Degens, E.T., Kempe, S., and Loliman, H., eds., Transport of Carbon and Minerals in Major World Rivers, Part 2, Proceedings of a workshop: Scientific Committee on Problems of the Environment/United Nations Education Program, International Carbon Unit, Hamburg, Federal Republic of Germany, Universität Hamburg, Geologisch-Paläontologisch Institut, Mitteilungen, v. 55, p. 55–84.

TUCKER, G.B., AND BARRY, R.G., 1969, Climate of the North Atlantic Ocean, in Landsberg, H.E., ed., World Survey of Climatology: Amsterdam, Elsevier, p. 193–257.

VAN ANDEL, T.H., 1967, The Orinoco delta: Journal of Sedimentary Petrology, v. 37, p. 297–310.

WIBERG, P.L., AND SMITH, J.D., 1983, A comparison of field data and theoretical models for wave-current interactions at the bed on the continental shelf: Continental Shelf Research, v. 2, p. 147–162.

YALIN, M.S., 1977, Mechanics of Sediment Transport: Oxford, Pergamon Press, 290 p.